Surface – Functionalized Inorganic Nanoparticles in Miniemulsion Polymerization

*Oliver Töpfer, Gudrun Schmidt-Naake**

Summary: Two inorganic cores, consisting of silica and titania, have been prepared via basic Stoeber synthesis. Those cores have been functionalized, using trimethoxysilyl propylmethacrylate (MPTMS) and introduced into a miniemulsion copolymerization system. The miniemulsion consisted of styrene (S) and 2-hydroxyethyl methacrylate (HEMA), styrene sulfonic acid (SSA) or aminoethyl methacrylate hydrochloride (AEMA) as comonomer in varying compositions. The morphology of the products has been investigated by SEM and dynamic light scattering (DLS) measurements. The composition of the products has been investigated by photoacoustic FTIR (PA-FTIR) spectroscopy and elemental analysis. Thermal properties have been determined by TGA and DSC analysis.

Keywords: functional precursors; miniemulsion; nanoparticles; polymer composites; reactive fillers

Introduction

In recent years, the combination of polymers and inorganic materials to polymer composites comes to steadily growing interest. Synergetic aspects such as chemical resistance or elasticity of the organic compounds and hardness, stability or interesting electrical and optical properties of the inorganic compounds offer an immense potential for new materials or applications. Hofman-Caris presented a detailed review about particle formation procedures as well as chemical coupling procedures that form core shell structures prior to 1994.[1]

A wide range of inorganics has been used as components in polymer composites. However, silica offers a broad and interesting variety of structural modifications such as layered silicates like montmorillonite, colloidal nanoparticles like Stoeber synthesis products or highly ordered architectures like siloxane or silsequioxane structures.[2,3]

A major problem is always the organic inorganic interface which does not interact per se and would lead to phase separation. While montmorillonite forms, depending on the reaction conditions, either intercalated or exfoliated composites with clearly separated phases, a phase separation in the composites with silica nanoparticles or siloxanes respectively silsesquioxanes is unrequested.[4,5]

Although first attempts used inorganic particles as fillers or additives without any covalent bonding, soon further development led into the covalent attachment of polymers onto sub-micrometer size particles.[6]

Therefore, miniemulsion polymerization turned out to be a suitable technique to produce polymer composites with an inorganic core and an organic shell.[7,8]

A following step was the copolymerization, using a second monomer, which enables the introduction of a secondary functionality into the emulsion bead. This leads to reactive fillers, which can be varied in composition and concentration of accessible functional groups at the particle

Institut für Technische Chemie, Technische Universität Clausthal, Erzstr. 18, 38678 Clausthal-Zellerfeld, Germany
Tel: (+49) 05323 722036 Fax: (+49) 05323 723655
E-mail: Gudrun.Schmidt@TU-Clausthal.de

surface. In recent publications, Landfester et al. reported about the synthesis and the uptake of fluorescent labelled poly(styrene-*co*-acrylic acid) core shell systems containing an magnetic iron oxide core for biomedical applications such as stem cell research.[9,10]

Few approaches have been done, using S in combination with Glycidyl methacrylate (GMA), HEMA or ω-amino alkyl methacrylates as functional comonomers.[11–13]

Besides the mentioned comonomers, SSA as well as AEMA has been used as comonomer in a miniemulsion copolymerization with styrene in our workgroup.[14]

Two different inorganic cores have been synthesized via basic Stoeber synthesis.[15,16] Both inorganic cores, the SiO_2 core as well as the TiO_2 core, have been functionalized with trimethoxysilyl propylmethacrylate (MPTMS) under condensation conditions. Scheme 1 shows a condensation and functionalization process exemplarily given on tetraethoxysilane (TEOS).

Those cores have been copolymerized under miniemulsion conditions using sodium dodecyl sulphate (SDS) as surfactant and potassium persulphate (KPS) as initiator with styrene as matrix monomer and HEMA, SSA and AEMA as comonomer. Apart from diffusion controlled effects in a swollen polymer shell, only those functional groups that are situated on the surface of the core shell particle are accessible for further reactions. To increase the specific surface area as well as the structural integrity of the core shell particle, the acrylate based crosslinker tetraethylene glycol diacrylate (TEGDA) has been introduced.

With this versatile reaction method we established an easy preparation scheme for reactive fillers with a broad variety of functionalities in adjustable concentration on the particle surface.

Experimental Part

Preparation and Functionalization of Silica Nanoparticles

Tetraethoxysilane (TEOS, 0.73 mol) is dissolved in absolute ethanol (1 000 mL) and is stirred at ambient temperatures. Via a syringe gaseous ammonia is added over a period of 30 minutes. After addition of ammonia, the dispersion is kept still for 6 hours.

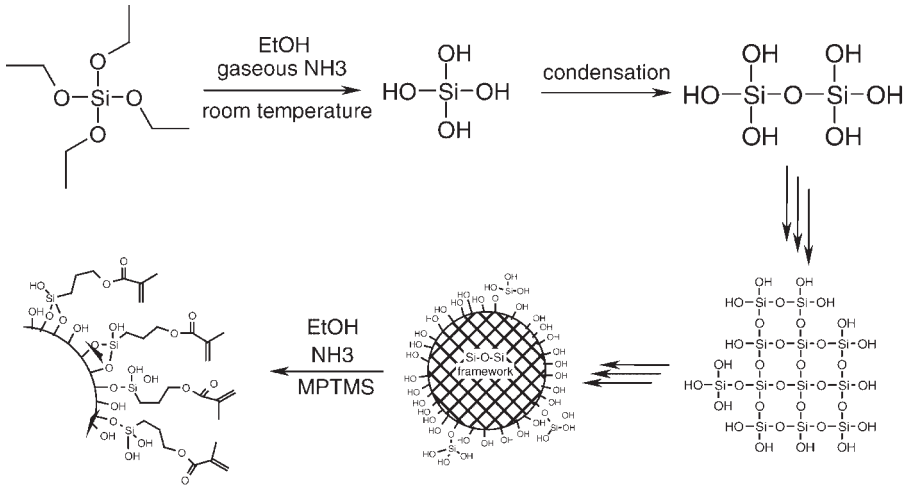

Scheme 1.
Condensation and functionalization process exemplarily shown on silica, using MPTMS for in-situ functionalization.

For functionalization the dispersion is stirred and MPTMS (4.0 mmol dissolved in 2 mL Ethanol) is added. The mixture is stirred for 12 hours. The solid content reaches 6 wt.-%.

Preparation and Functionalization of Titania Nanoparticles

The preparation and functionalization of TiO_2 follows the procedure given above, using Tetraethoxytitanate instead of TEOS for the condensation process.

Miniemulsion Polymerization Setup

1.9 wt.-% of SDS is dissolved into a dispersion of 1 g inorganic compound (corresponds to 0.47 mmol functional groups) in ethanol. The monomer mixture of S/functional monomer/TEGDA is added. The system is diluted with ethanol to an overall volume of 95 mL. The collective monomer concentration is set to 0.3 mol/L. The mixture is emulsified by ultrasonification (90 sec.) and transferred into a double mantle heating reactor, equipped with a mechanical stirrer and a nitrogen inlet. The emulsion is heated to 70 °C. KPS (0.5 wt.-% resp. the amount of monomer) is dissolved in 5 mL deionized water and added to the preheated emulsion. Reaction time is set to 60 minutes.

Analytical Equipment

Photoacoustic-FTIR has been done, using the FTS 7000 series machine from DIGILAB, equipped with a photoacoustic detector model 300 from MTEC. Helium was used as purge gas and the software Win-IR-Pro was used for data analysis.

Dynamic light scattering measurement has been done, using the Photon Cross-correlation Spectroscopy (PCCS) machine NANOPHOX provided by SYMPATEC. Data analysis has been done, using the system software Windox 5.2.2.0 from SYMPATEC.

Elemental analysis has been done on a Vario EL2 machine from ELEMENTAR. The elements C, H, N, S has been detected with a thermal conductivity detector. Oxygen has been detected with an infrared detector. Sulfanilic acid and benzoic acid have been used for calibration.

Thermogravimetrical measurements have been done on a TGA 850 from METTLER TOLEDO. Temperature range was 25 °C to 850 °C with a temperature ramp of 20 K/min.

Scanning Electron Microscopy has been done on a Gemini 982 from ZEISS. For high magnification, Cr has been used as sputter medium.

Results

Inorganic Particle Formation and Functionalization

The particle formation follows the well known Stoeber synthesis in basic ethanol. A time resolved nanoparticle formation has been observed in the case of silica. The result is given in Figure 1 as particle size versus condensation time curve.

The fitted curves in Figure 1 show that the particle growth process reaches a limit at 180 minutes. To ensure a full conversion, a reaction time of 6 hours seems to be sufficient for particle formation.

The nanoparticle functionalization using MPTMS follows in situ. Figure 2 shows the particle size distribution of silica and titania nanoparticles before and after functionalization. The mentioned polydispersity index (PDI) represents the quotient of X_{90} divided by X_{50}.

The average particle size increases in both cases by a few nm due to the attached methacryloyl groups. However, no aggregation is observed during particle formation or functionalization. Thermogravimetrical analysis of the washed and dried product indicates 9 wt.-% of organic compound covalently bond onto the particle surface which can be calculated to a number of 200,000 methacryloyl groups on the surface of a particle with a diameter of 100 nm or 0.47 mmol methacryloyl groups per gram inorganic compound.

The successful attachment of MPTMS to silica or titania can be shown in the infrared spectra of the washed and dried silica and titania, given in Figure 3.

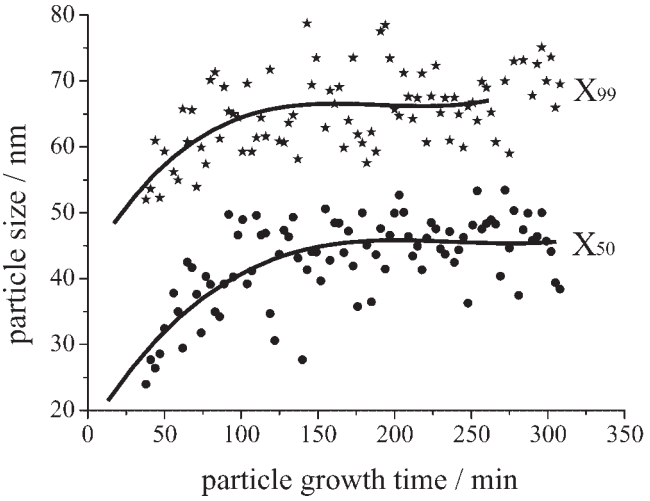

Figure 1.
Particle size as a function of time given for the condensation of TEOS in basic ethanol. X_{50} value represents maximum particle size, which 50% of the particles underrun; X_{99} represents maximum particle size, which 99% of the particles underrun.

The attached methacryloyl group can be seen at the cumulative vibrations of the ester group at 1 295 cm^{-1} and 1 460 cm^{-1} as well as the double bond stretching at 1 721 cm^{-1}. Furthermore, significant framework vibrations are visible, for silica in the range of 750 cm^{-1} to 1 250 cm^{-1} and for titania below 1 000 cm^{-1} as broad signals.

Polymer Composite Properties

The functionalized nanoparticles were copolymerized in a miniemulsion system of S and a variety of functional comonomers.

The miniemulsion polymerization products were washed with acetone to remove soluble components from the polymer composite. Spectroscopic characterization of the dried products was done using PA-FTIR spectroscopy. This method allows a convenient and fast spectroscopic analysis.

Figure 4 shows the PA-FTIR spectra of poly(S-*co*-HEMA) polymer composite of functionalized silica with increasing HEMA concentration.

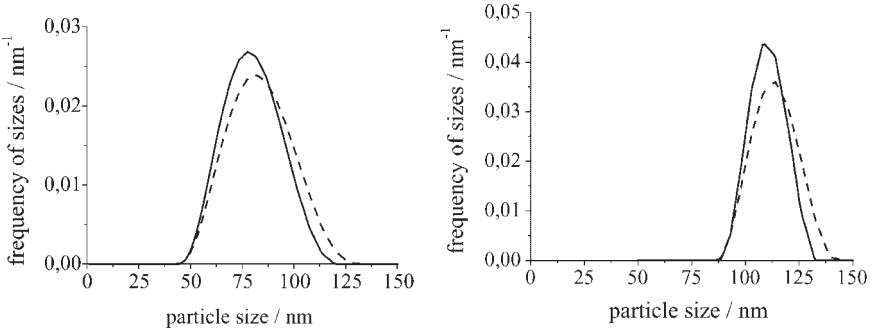

Figure 2.
left: Particle size distribution of non modified silica (solid line) with an average particle size of 77 nm (PDI 1.2) and MPTMS modified silica (dashed line) with an average particle size of 79 nm (PDI 1.4).; right: Particle size distribution of non modified titania (solid line) with an average particle size of 112 nm (PDI 1.1) and MPTMS modified titania (dashed line) with an average particle size of 115 nm (PDI 1.4).

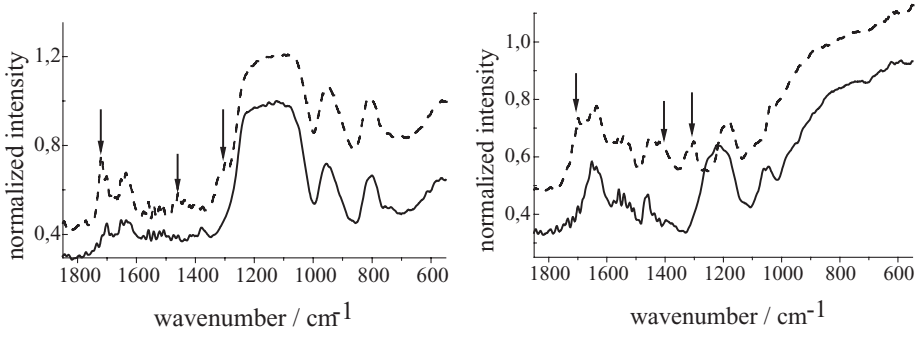

Figure 3.
left: Photoacoustic infrared spectra of non modified silica (solid line) and MPTMS modified silica (dashed line).; right: Photoacoustic infrared spectra of non modified titania (solid line) and MPTMS modified titania (dashed line).

The variation of the functional monomer concentration is reflected in the PA-FTIR spectra of the miniemulsion products. An increasing of the HEMA content in the polymer composite can be seen at the significant carbonyl stretching band at 1 600 cm^{-1} which increased in the spectra from product 1 to product 3 with increasing of the HEMA content in the monomer composition. Nevertheless, next to the typical copolymer bands for poly(S-*co*-HEMA), significant silica core bands are visible in all spectra. The monomer composition as well as the product composition after copolymerization is given in Table 1.

The polymer composition has been calculated using the copolymerization parameters of HEMA and S ($r_S = 0.44$ and $r_{HEMA} = 0.54$).[17] The influence of the crosslinker TEGDA has been neglected in both cases, the preparation of the copolymer and of the polymer composite. Nevertheless, a good agreement within the error margin has been found for the typical copolymerization with HEMA contents below 20 mol% in the monomer

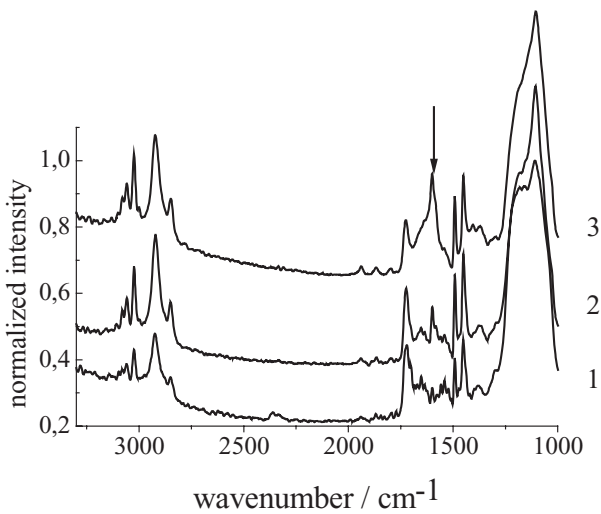

Figure 4.
PA-FTIR spectra of S-*co*-HEMA polymer composite of functionalized silica with increasing HEMA content in the product. 1: HEMA content 7.1 mol%; 2: HEMA content 11.1 mol%; 3: HEMA content 19.8 mol%.

Table 1.
Data of monomer and polymer composition as well as particle size and polydispersity index (PDI) of the particle size distribution.

	monomer system	feed composition [mol%]	polymer composition [mol%]	Conversion [%]	Particle size X_{50} [nm]	PDI (X_{90}/X_{50})
SiO_2	S/SSA/TEGDA	93,5/**4,9**/1,6	95,6/**2,6**/1,8	90	113	1,2
		88,5/**9,8**/1,6	86,5/**12,2**/1,3	95	151	1,4
		78,7/**19,7**/1,6	80,2/**17,6**/1,8	97	175	1,2
	S/AEMA/TEGDA	93,5/**4,9**/1,6	84,9/**13,2**/1,8	96	112	1,6
		88,5/**9,8**/1,6	80,1/**18,1**/1,8	98	124	1,3
		78,7/**19,7**/1,6	68,5/**29,6**/1,9	97	135	1,2
	S/HEMA/TEGDA	93,5/**4,9**/1,6	91,1/**7,1**/1,8	80	96	1,4
		88,5/**9,8**/1,6	87/**11,1**/1,8	76	-	-
		78,7/**19,7**/1,6	78,4/**19,8**/1,9	70	149	1,2
-	S/SSA/TEGDA	93,5/**4,9**/1,6	95,8/**2,6**/1,6	95	-	-
		88,5/**9,8**/1,6	90,8/**8,1**/1,1	97	143	1,2
		78,7/**19,7**/1,6	79,6/**19,2**/1,2	94	173	1,3
-	S/AEMA/TEGDA	93,5/**4,9**/1,6	96,7/**1,6**/1,8	96	123	1,2
		88,5/**9,8**/1,6	93,3/**4,9**/1,8	92	125	1,2
		78,7/**19,7**/1,6	-	97	139	1,3
-	S/HEMA/TEGDA	93,5/**4,9**/1,6	87/**11,4**/1,6	78	196	1,3
		88,5/**9,8**/1,6	81,7/**16,8**/1,5	80	216	1,3
		78,7/**19,7**/1,6	74,2/**24,1**/1,7	75	191	1,2
TiO_2	S/SSA/TEGDA	93,5/**4,9**/1,6	90,7/**9,1**/0,2	92	494	1,8
		88,5/**9,8**/1,6	85,7/**14,1**/0,2	90	317	1,7
		78,7/**19,7**/1,6	77,4/**22,3**/0,3	86	357	1,6
	S/AEMA/TEGDA	93,5/**4,9**/1,6	93,5/**4,9**/1,6	98	141	1,5
		88,5/**9,8**/1,6	88,5/**9,8**/1,6	98	146	1,7
		78,7/**19,7**/1,6	78,7/**19,7**/1,6	97	158	1,5

feed composition (Figure 5). Contrary to the copolymerization, the formation of the polymer composite does not follow the predicted copolymerization diagram. Especially for higher HEMA contents, the polymer composition deviates from the predicted copolymerization behaviour.

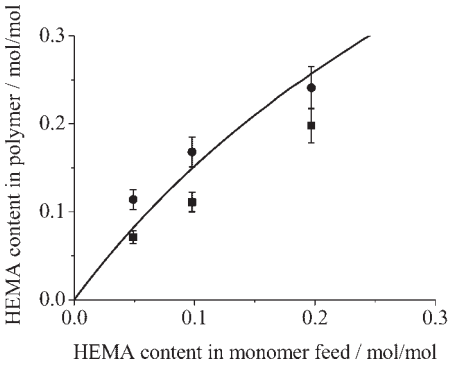

Figure 5.
HEMA content in the polymer composite (squares) and HEMA content in the copolymer (dots) as function of the HEMA content in the monomer feed. The copolymer composition calculated from $r_S = 0.44$ and $r_{HEMA} = 0.54$ is given as reference (solid curve).

This leads to the assumption, that the inorganic nanoparticle influences the copolymerization in the emulsion droplet. Besides the functional methacryloyl groups, each nanoparticle provides many hydroxyl groups at the surface. Those hydroxyl groups at the surface could interact with the hydroxyl groups of the added monomer in a way of repulsion. Therefore, the monomer composition in the emulsion droplet changes which could lead to a different polymer composition in the organic inorganic copolymerization product.

Due to the fact that HEMA as a component in the copolymerization decreases the thermal stability, the decreasing of the thermal degradation temperature for both, the polymer composite and the copolymer, with an increasing HEMA content is understandable. Nevertheless, the inorganic core in the polymer composite seems to influence the thermal stability positively. An increase of 15 K in the thermal stability of the polymer composite is observed (Figure 6).

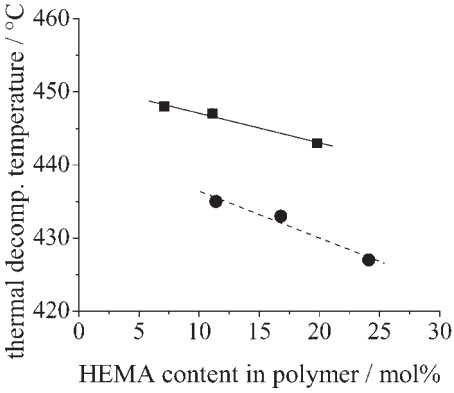

Figure 6.
Thermal decomposition temperature of the polymer composite (squares, solid line) and the copolymer (dots, dashed line) as function of the HEMA content in the product.

The morphology of the S-*co*-HEMA polymer composite exhibits a typical miniemulsion product of spherical particles with a narrow particle size distribution (Figure 7).

Figure 8 shows the PA-FTIR spectra of the poly(S-*co*-AEMA) polymer composite with functionalized silica at increasing AEMA concentration.

The conversion of the 2-aminoethyl methacrylate hydrochloride monomer to the free amino group in the polymer composite has been conducted completely which is clearly visible at the shift of the amino-hydrochloride band (spectrum 4; broad at 2 700 cm^{-1} to 2 900 cm^{-1}) to the free amino group vibration band (spectra 1 to 3; broad at 3 200 cm^{-1} to 3 500 cm^{-1}). The increasing band intensities of the amino group vibration as well as the carbonyl group (weak, sharp at 1 650 cm^{-1}) indicate the growing incorporation of the functional monomer into the polymer composite compound.

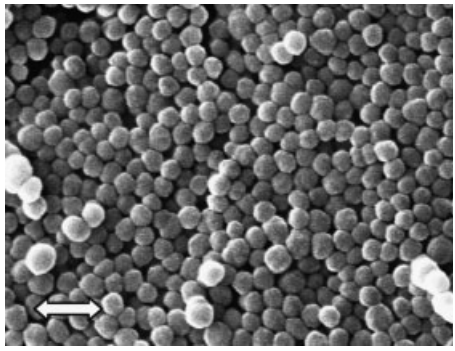

Figure 7.
SEM image of S-*co*-HEMA polymer composite (HEMA content 19.8 mol%) with an average particle size of 150 nm. Arrow size is 500 nm.

Figure 9 shows the concentration of the functional monomer, HEMA and AEMA, in the polymer composite as a function of the functional monomer content in the feed.

Significantly more AEMA is integrated into the polymer composite than HEMA is integrated in the composite. Furthermore, more AEMA is integrated into the polymer composite than it is provided in the monomer feed. However, a tailoring of compositions with up to 30 mol% AEMA content or up to 20 mol% HEMA content in the polymer composite is possible and easily accessible.

The average particle size as well as the particle size distribution of the prepared lattices was investigated under reaction state concentration using a novel dynamic light scattering method.[18,19] Table 1 summarizes relevant data of the prepared products. Furthermore, the composition of the monomer feed as well as the composition of the polymer is given in Table 1. The polymer composition has been calculated from elemental analysis data.

The particle sizes of the minimeulsion product increase in all samples compared to the silica and titania precursors. Furthermore a low PDI is found which indicates an extensive incorporation of the silica and titania cores into the miniemulsion droplet.

The incorporation of functionalized titania into a S/SSA system follows equal schemes, given above.

Figure 10 shows the PA-FTIR spectra of the polymer composite with increasing SSA content in the product indicated at the vibrations of the sulfonic acid group at 1 650 cm^{-1} (medium, sharp) and at 3 450 cm^{-1} (medium, broad)

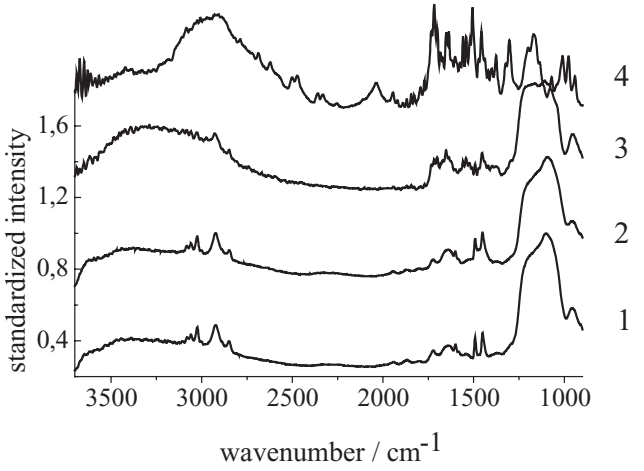

Figure 8.
S-*co*-AEMA polymer composite with functionalized silica and increasing AEMA content in the product. 1: AEMA content 13.2 mol%; 2: AEMA content 18.1 mol%; 3: AEMA content 29.6 mol%; 4: 2-Aminoethyl methacrylate hydrochloride monomer.

The SEM image of the miniemulsion product (Figure 11) shows spherical particles with a narrow particle size distribution and an average particle size of 150 nm. This confirms the results from the dynamic light scattering measurements.

The thermal stability of the prepared poly(S-*co*-SSA) polymer composites with silica and titania decreases with increasing SSA content. However, the prepared copolymers of poly(S-*co*-SSA) show significant higher decomposition temperatures which are not affected by the increasing SSA content in the product. Figure 12 shows the thermal decomposition temperature as a function of the SSA content in the miniemulsion polymerization product.

The polymer composites show a decreased thermal stability compared to the S-*co*-SSA copolymer. This might be an effect of different thermal conductivities at the organic – inorganic interface which interferes with the polymer matrix. Furthermore, monomer –specific interactions between the inorganic surface and the

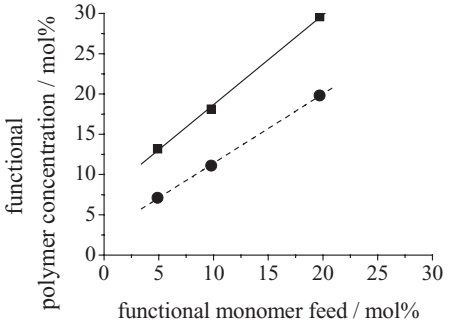

Figure 9.
Functional monomer concentration of HEMA (dots, dashed line) and AEMA (squares, solid line) in the polymer composite versus functional monomer concentration in the monomer feed.

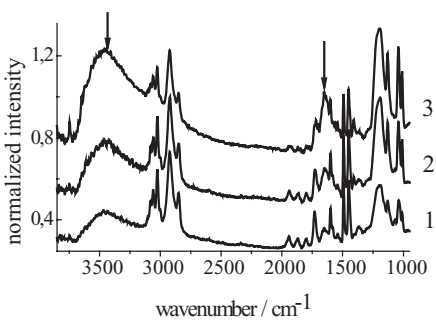

Figure 10.
S-*co*-SSA polymer composite with functionalized titania and increasing SSA content in the product. 1: SSA content: 9.1 mol%; 2: SSA content: 14.1 mol%; 3: SSA content: 22.3 mol%.

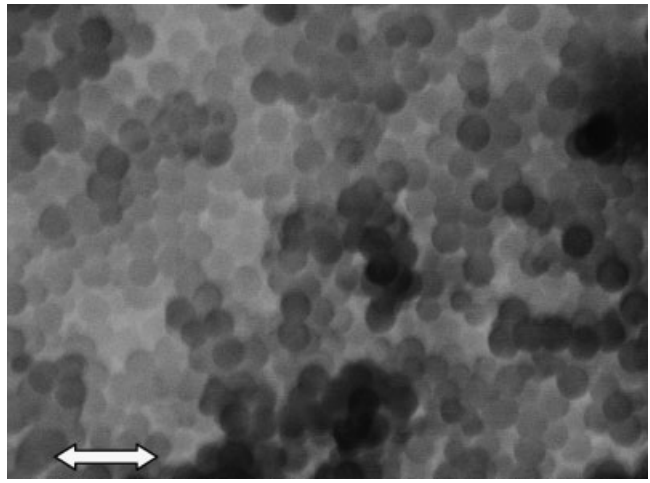

Figure 11.
SEM image of S-*co*-SSA polymer composite of functionalized silica (SSA content 12.2 mol%) with an average particle size of 150 nm. Arrow size is 500 nm.

copolymer might cause the different thermal behaviour with an increasing SSA content in the composite.

The ion exchange capacity (IEC) of the polymer composite containing SSA has been determined. Figure 13 gives the theoretical IEC and the obtained IEC as function of the SSA content in the polymer composite with silica.

It is clearly visible, that the IEC is increasing with increasing SSA content in the polymer composite. The theoretical IEC represents the maximum IEC if all SSA groups are accessible. Hence, a reduced IEC for the real accessible SSA groups is expected. Nevertheless, at least 75% of the SSA groups are accessible (sample with 17.6 mol% SSA content). Due to the effect that the TEGDA increases the specific surface area and produces highly porous particles, this high amount of available SSA groups can be achieved.

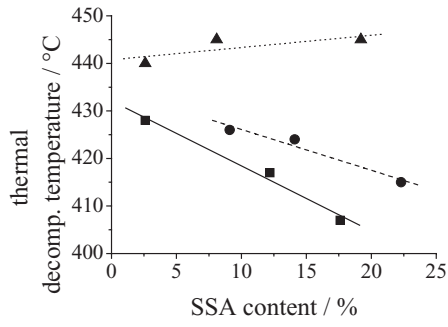

Figure 12.
Thermal stability of S-*co*-SSA polymer composite with silica (squares, solid line), titania (dots, dashed line) and S-*co*-SSA polymer (triangles, dotted line) for comparison.

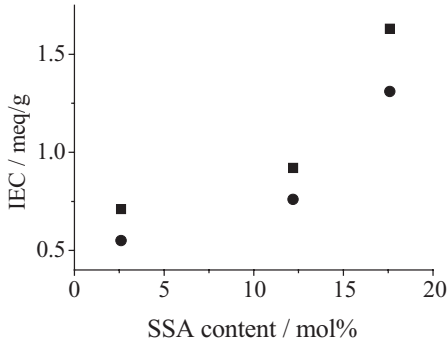

Figure 13.
Ion exchange capacity (IEC) of S-*co*-SSA polymer composite with silica. Expected IEC from EA composition calculation (squares) and obtained IEC from equivalence titration (dots).

Conclusion

It has been shown that the preparation of functionalized organic/inorganic polymer composites, consisting of silica or titania cores and an organic copolymer shell was successful. Therefore, the inorganic cores have been prepared by basic Stoeber synthesis, functionalized using MPTMS and embedded into a miniemulsion copolymerization system. The used monomers for copolymerization were S and HEMA or AEMA and SSA in a variation of 5 mol% over 10 mol% to 20 mol% functional monomer related to S.

In the case of poly(S-*co*-HEMA) polymer composites with silica, the HEMA content could be varied from 8 mol% to 20 mol% which could be adjusted in the monomer feed. However, higher incorporation rates than poly(S-*co*-HEMA) polymer composites could be achieved in the poly(S-*co*-AEMA) system with either silica or titania.

Dynamic light scattering measurements of the miniemulsion lattices prove the successful incorporation of the inorganic cores into the miniemulsion droplet. All silica based polymer composites show particle sizes between 120 nm and 150 nm with a low PDI, whereas the silica precursor itself showed an average particle size of 79 nm. Hence, all silica nanoparticles have been incorporated into the emulsion droplet and each droplet contains only one silica particle. This can be proved by the SEM image of the composite.

In the case of the titania based polymer composites, the samples with poly(S-*co*-AEMA) show average particle sizes of 140 nm to 160 nm. Here, the polymer shell has been formed around one nanoparticle in the emulsion droplet.

The titania based polymer composites with poly(S-*co*-SSA) show rather large particles with particle sizes of 300 nm to 500 nm. In this case, it is possible that two or more titania particles could have entered the emulsion droplet. Still the product remains stable and no aggregation has been observed. However the IEC measurements confirm the integration of SSA into the polymer composite. The accessible SSA groups reach up to 75% of the calculated maximum due to the fact that the added crosslinker TEGDA increases the specific surface area by forming porous and highly swellable shells around the inorganic core of this system.

The presented three step method of inorganic particle preparation, consequent functionalization and finally embedding into a miniemulsion copolymerization system offers an easy way to prepare core shell particles with a wide range of functionalities at the surface. Those products inherit a high potential as reactive filler materials in advanced polymers composites.

[1] C. H. M. Hofman-Caris, *New J. Chem.*, **1994**, *18*, 1087.
[2] A. Shimojima, K. Kuroda, *Chem. Lett.*, **2000**, 1310–1311.
[3] J. Wen, G. L. Wilkes, *Chem. Mater.*, **1996**, *8*, 1667–1681.
[4] M. Biswas, S. S. Ray, in: New Polymerization Techniques and Synthetic Methodologies, Vol. 155 of Advances in Polymer Science, Springer Verlag 2001, p. 167–234.
[5] M. Biswas, S. S. Ray, *Polymer*, **1998**, *39*, 6423–6428.
[6] E. Bourgeat-Lami, *J. Nanosci.Nanotech.*, **2002**, *2*, 1–24.
[7] E. Bourgeat-Lami, *Polymer*, **1995**, *36*, 4385–4389.
[8] P. Espiard, A. Guyot, *Polymer*, **1995**, *36*, 4391–4395.
[9] V. Holzapfel, M. Lorenz, C.-K. Weiss, H. Schrezenmeier, K. Landfester, V. Mailander, *J. Phys. Cond. Matter*, **2006**, 18(38), 2581–2594.
[10] M. Lorenz, V. Holzapfel, A. Musyanovych, K. Nothelfer, P. Walther, H. Frank, K. Landfester, H. Schrezenmeier, V. Mailander, *Biomaterials*, **2006**, *27*(14), 2820–2828.
[11] E. Bourgeat-Lami, J. Lang, *Macromol. Symp.* **2001**, *169*, 89–91.
[12] P. Innocenzi, T. Kidchob, T. Yoko, *J. Sol-Gel Sci. And Technol.*, **2005**, *35*, 225–235.
[13] Z. Zeng, J. Yu, Z.-X. Guo, *J. Polym. Sci. Part A*, **2004**, *42*, 2253–2262.
[14] I. Grabs, G. Schmidt-Naake, *publication in progress*.
[15] W. Stöber, A. Fink, E. Bohn, *J. Coll. Int. Sci.*, **1968**, *26*, 62–69.
[16] P. Philipse, A. Vrij, *J. Coll. Int. Sci.*, **1989**, *128*, 121–136.
[17] J. Brandrup, E. H. Immergut, in: Polymer Handbook, 3rd Edition, Wiley-Interscience Publication, p. II–251; New York, Brisbane, Chichester, Toronto, Singapore.
[18] W. Witt, L. Aberle, H. Geers, *Particlulate System Analysis*, **2003**, Harrogate.
[19] W. Witt, L. Aberle, H. Geers, Partec, **2004**.

